North Sea FLOW Measurement Workshop

Paper 3.1

Ultrasonic Flare Gas Flow Meter Techniques for Extremes of High and Low Velocity Measurement and Experience with High CO2 Concentration

Jed Matson
GE Sensing & Inspection Technologies

Lei Sui
GE Sensing & Inspection Technologies

Toan H. Nguyen
GE Sensing & Inspection Technologies

TÜV SÜD

nel technology for life

Ultrasonic Flare Gas Flow Meter Techniques for Extremes of High and Low Velocity Measurement and Experience with High CO2 Concentration

Jed Matson, GE Sensing & Inspection Technologies
Lei Sui, GE Sensing & Inspection Technologies
Toan H. Nguyen, GE Sensing & Inspection Technologies

1 INTRODUCTION

The ultrasonic transit time gas flowmeter has been established as the preferred method for Flare Gas flow measurement with more than 3000 units installed worldwide in process plants and refineries, on and offshore. New requirements around total emissions have been, or are being, implemented around the world and this presents additional technical challenges for ultrasonic flowmeters in the areas of (1) extremely low flare flow rates (0.3 m/s and below) during normal, or base load flaring, (2) extremely high flare flows (80 m/s and above) during emergency flaring and (3) measuring the flow rate of gas with a high CO_2 concentration. Low flare flows are influenced and asymmetric due to convection flow and stratification; High flare flows introduce soaring flow noise, cause ultrasonic beam drift and thus deteriorate ultrasonic signal quality. High CO_2 gas concentration can drastically attenuate ultrasonic energy.
In this paper, the uncertainty of flow rate at low flow is examined and demonstrated in the typical large diameter flare gas pipes. Techniques for improving the uncertainty of flow at low velocity, both for required resolution, and for better area averaging of asymmetric flow profile are presented. The ultrasonic signal propagation in (flare) gas has been studied, the beam drift due to gas flow has been investigated and improvements from both mechanical and transducer perspectives have been made to compensate for these two problems. An improved version of the flare gas ultrasonic meter has been developed to demonstrate the accurate measurement of air flow up to 123.7 m/s. Testing data have been presented for two typical configurations, Bias 90 and Diagonal 45, in comparison with a Venturi reference meter. The overall accuracy of the new flare meter is demonstrated to be 3-4%, and the relative standard deviation of the meter readings is within 1.2%. In addition specific applications of the flare gas flowmeter to gases with high CO_2 concentration, as high as 100%, are examined and the solutions are described

2 HIGH VELOCITY FLOW

Flare systems are primarily installed for safety purposes in chemical, petrochemical, refining, and other plants. These flare systems are used to vent and burn off hydrocarbons and other unwanted gases under routine and emergency conditions, such as an unexpected shutdown. Today there is an international awareness to measure and monitor flare gas flow for both environmental and economical reasons [1][2][3]. The measurement of flare gas helps to comply with environmental regulations, identify points of leakage, and reconcile plant mass balance.
Flare gas flow measurement itself is challenging mainly due to factors such as: unsteady flow velocity, pressure fluctuations, variable composition, aggressive chemicals in the gas, potential high temperature excursions and a wide-range of flow rates. In particular, it requires instrumentation to be capable of measuring gas flow over a wide range of velocities: from 0.03 m/s low flow, through 0.15-0.5 m/s for most normal operations, and up to 80 m/s and above during emergency flaring.
In the early 1980s, a flare gas ultrasonic flowmeter was first jointly developed by Panametrics (now GE Sensing) and Exxon (now ExxonMobil) in Baytown, Texas, USA. [1]. Since then, ultrasonic flowmeters have been gaining more and more popularity for flare gas measurement, mainly because of its high turndown ratio, its relatively low installation and maintenance costs, its capability of handling unsteady flows, and its independence from gas composition. Today, the ultrasonic flow meter is the accepted technology for monitoring flare gas, with more than 3,000 installations worldwide.
Although flare gas ultrasonic flowmeters have evolved with many improvements over the past 25 years, one of the remaining technical challenges is to deal with extremely high flow velocity up to 80 m/s and above. Such high flare gas flows can occur during a process shutdown when all the process gases need to be flared. A poor signal quality at high flow velocities, usually quantified by low signal-to- noise ratio (SNR), is due to such factors as beam drift, greatly-increased noise level, and

turbulence-related attenuation, that cause scattering and distortion of ultrasonic signals [4]. As a result, flare gas ultrasonic flowmeters available on the market today offer the maximum velocity typically of 85 m/s – 100 m/s [5][6].
An ultrasonic flowmeter has been developed and tested for high-velocity gas measurement up to 123.7 m/s in air. The enabling technologies behind this new development are design of the transducer dimensions, transducer separation and operating frequency, and the implementation of a recovery angle to the downstream transducer. Testing results obtained from a wind tunnel in the Energy and Propulsion Technologies Laboratory at the GE Global Research Center located in Niskayuna, NY is presented. The accuracy of the new meter is demonstrated to be better than 3-4% with reference meter uncertainty included, and the relative standard deviation of the new meter is within 1.2%.

2.1 Methodology: Design of Transducer Dimensions, Separation, and Frequency

Using ultrasound to measure flow velocity has been a well-known technique for decades [7]. Transit-time ultrasonic flowmeters take advantage of a simple principle, called “time of flight”, as illustrated in Fig. 1. Specifically, the time it takes for an ultrasonic signal to travel against the flow (i.e., upstream), t_{up}, is longer than the time it takes with the flow (i.e., downstream), t_{dn}. The difference between upstream and downstream transit times, Δt, is directly proportional to the flow velocity as follows [8][9]:

$$V = \frac{P}{2\cos\theta}\left(\frac{1}{t_{dn}} - \frac{1}{t_{up}}\right) = \frac{P}{2\cos\theta}\left(\frac{\Delta t}{t_{dn}\ t_{up}}\right), \qquad (1)$$

Where V is the flow velocity to be measured, P is the ultrasonic path length, and θ is the acute angle between the ultrasonic path and the axis of the flowcell or pipe section.

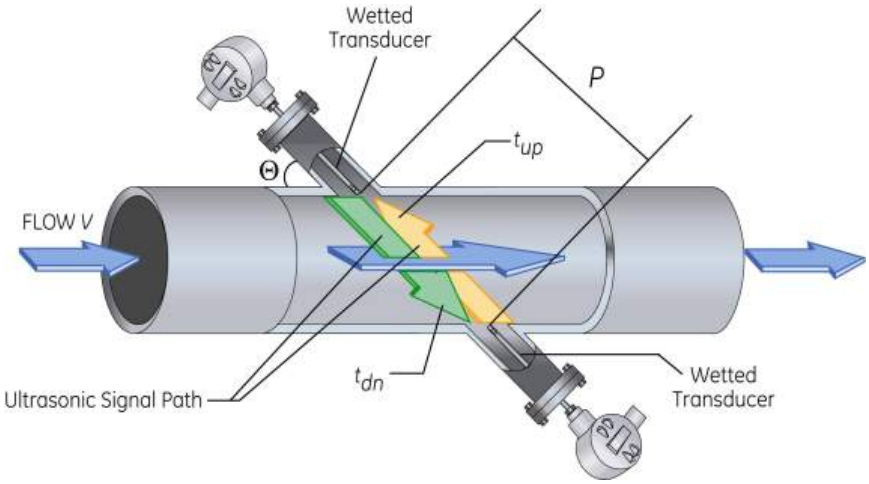

Figure 1. The operating principle of a transit-time based ultrasonic flowmeter.

From Eq. (1), it can be seen that the measurement strongly depends on the timing of t_{up}, t_{dn}, and Δt. The measurements of t_{up}, t_{dn}, and Δt rely on the quality of the received ultrasonic signal, i.e., signal-to-noise ratio (SNR).
For linear ultrasound propagation, there exist near-field and far-field regions, with the latter beginning at the so-called Rayleigh distance [10].

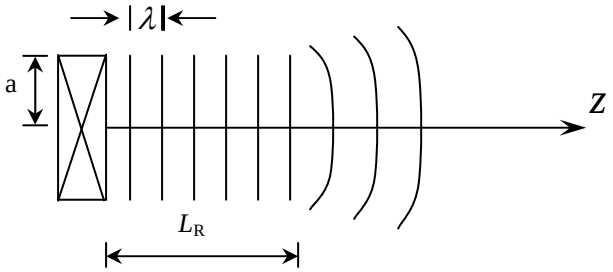

Figure 2. Ultrasound propagation in a medium across both near field and far field nominally separated by Rayleigh Distance, L_R.

In the far field, the pressure amplitude at location z (which is measured along the transducer axis with $z = 0$ starting at the transducer surface), *P* (*z*), can be approximately written as [11]:

$$P(z) = K_0 \frac{a^2}{z} e^{-\alpha z}, \qquad (2)$$

Where K_0 is a constant determined by the driving amplitude of the transducer, efficiency of the transducer, and the medium in which ultrasound is propagating, and α is the ultrasonic attenuation coefficient in units of neper/m or dB/m. The ultrasonic attenuation coefficient depends on the medium in question and is typically a function of the ultrasonic frequency by the power law as:

$$\alpha = \alpha_0 f^n, \qquad (3)$$

In which α_0 and *n* are two coefficients used to describe this function. In practice, both α_0 and *n* could be obtained by measuring ultrasound pressure at different frequencies and distances.

Substituting Eq. (3) into Eq. (2), we obtain:

$$P(z) = K_0 \frac{a^2}{z} e^{-\alpha_0 f^n z}. \qquad (4)$$

Eq. (4) indicates that to increase the ultrasonic signal amplitude, it is desirable to have transducers with a large radius (or diameter), to keep the separation of the transducer pair close, and to select a relatively low ultrasonic frequency. In reality, the transducer dimensions are limited by the cost of the transducers, the mechanical arrangement associated with the transducers, and the openings in the flowcell; the larger openings on the pipe tend to disturb the local flow profile. Similarly, the separation of the transducers is restricted by the accuracy requirement at low flow rates. Finally, the selection of an ultrasonic frequency is a trade-off between maximizing resolution and minimizing attenuation. Taking the above compromises into consideration, the transducer design has a radius of 0.375" and a frequency of 100 kHz (refer to [13] for more transducer details), and a separation of the transducer pair of ~6.5 to 7.8".

2.2 Recovery Angle

One difficulty with ultrasonic measurement of high velocity flare is ultrasonic beam drift. The high velocity will blow the ultrasonic signal away and this will result in a miss of the "perfectly aligned" targeted receiving transducer. We can calculate the downstream beam drift angle γ due to flow velocity *V* in a gas medium characterized by its speed of sound *c* as follows:

$$\gamma = \theta - \arctan\left(\frac{c\sin\theta}{c\cos\theta + V}\right) = \theta - \arctan\left(\frac{\sin\theta}{\cos\theta + M}\right), \qquad (5)$$

Where θ is as defined above, i.e., the acute angle between the ultrasonic propagation and flow directions, and $M = V/c$ is the Mach number. Similarly, the upstream beam drift angle γ can be derived as follows:

$$\gamma = \begin{cases} \theta - \arctan\left(\dfrac{\sin\theta}{\cos\theta - M}\right) & for \quad M < \cos\theta \\ \theta - 90^0 & for \quad M = \cos\theta \\ \theta - \arctan\left(\dfrac{\sin\theta}{\cos\theta - M}\right) - 180^0 & for \quad M > \cos\theta \end{cases}. \qquad (6)$$

From Fig. 3 it is evident that the upstream ultrasonic beam drift is typically more severe than the downstream beam drift. That is, for the same Mach number, the absolute upstream beam drift angle is larger than the downstream beam drift angle. The flowmeter is eventually limited by the upstream signal when it comes to measuring extremely high flows [4]. The upstream signal is decreased by

about 6 dB due to the beam drift alone at a flow of around 100 m/s in air, while there other adverse effects imposed by the high flow, such as high flow noise and Doppler shift [14].
A recovery angle can be implemented to offset the beam drift effect, as demonstrated in Reference [5], where recovery angles were applied to both downstream and upstream transducers. It should be noted that the accurate implementation of recovery angle on both transducers could be either time consuming, particularly in the field during the hot/cold tap procedures, or costly, or both. Since the above calculation shows beam drift is primarily on the upstream signal generated by the downstream transducer, we implement the recovery angle on the downstream transducer by rotating it about 6^0 in favour of the high flow velocity. Here 6^0 is chosen as a compromise between high-flow and low-flow measurements.

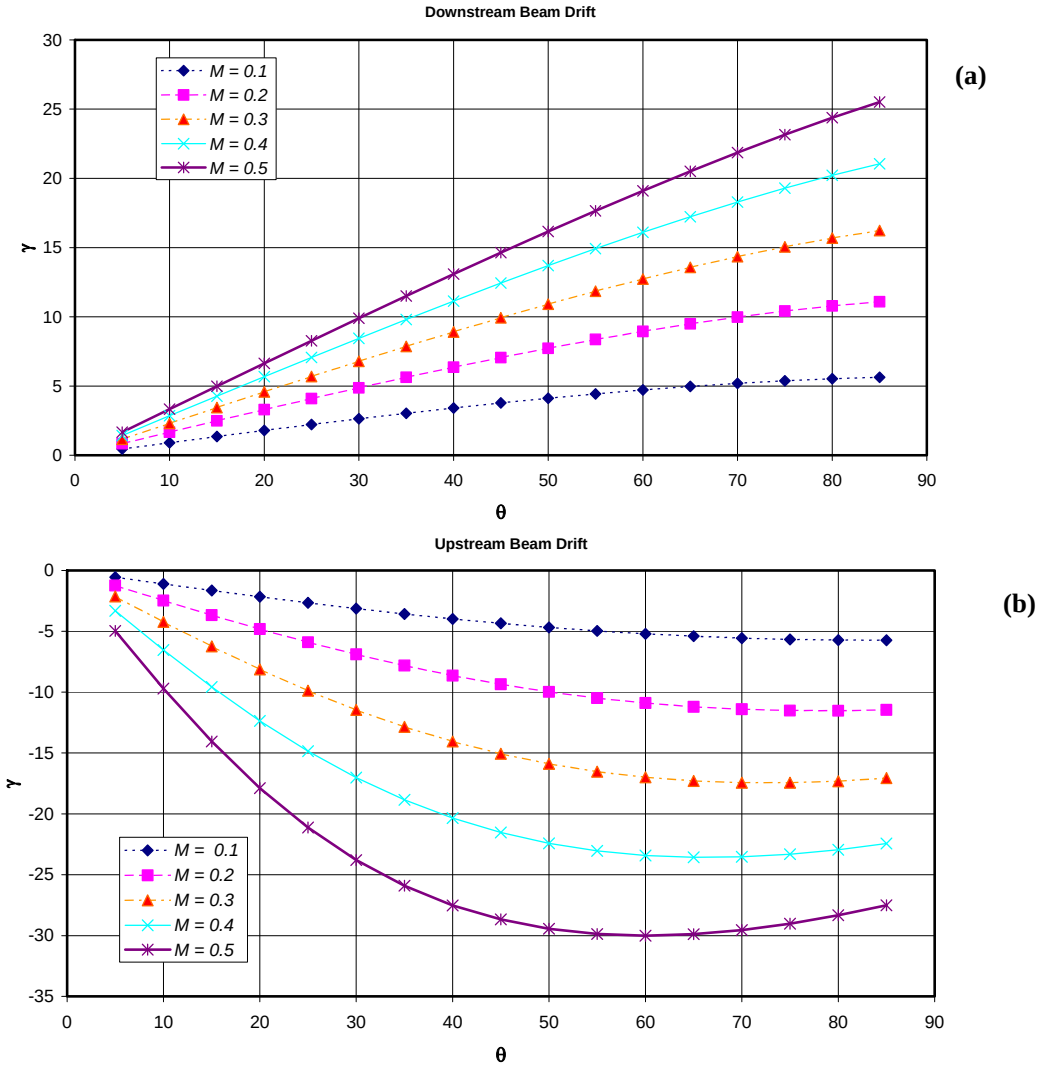

Figure 3. (a) Downstream and (b) Upstream ultrasonic beam drift angle as a function of ultrasonic path angle at different Mach numbers.

2.3 Increasing SNR

Another method we use to increase the SNR is to electrically tune the transducer. This is common for transducer design, and has been abundantly discussed in literature and thus omitted here for conciseness.

2.4 Final Conceptual Design

The final conceptual design of the high velocity flare gas ultrasonic meter is schematically shown in Fig. 4. The path length between transducers is kept relatively short, about 6 to 7.8", the path angle is chosen to be about 45^0, and the 6^0 recovery angle is implemented to the downstream transducer only. Two steel flow cells were manufactured for testing based on the above design. One is called Bias 90 (refer to Fig. 5 (a)) where the two transducers are placed on the same side of the flowcell, and the other is called Diagonal 45 (refer to Fig. 5 (b)) where the two transducers are placed from two different sides of the flowcell. It should be noted the transducers are rigidly mounted to withstand vibration, and that testing and calculation have shown the system to endure up to 120m/s and well beyond.

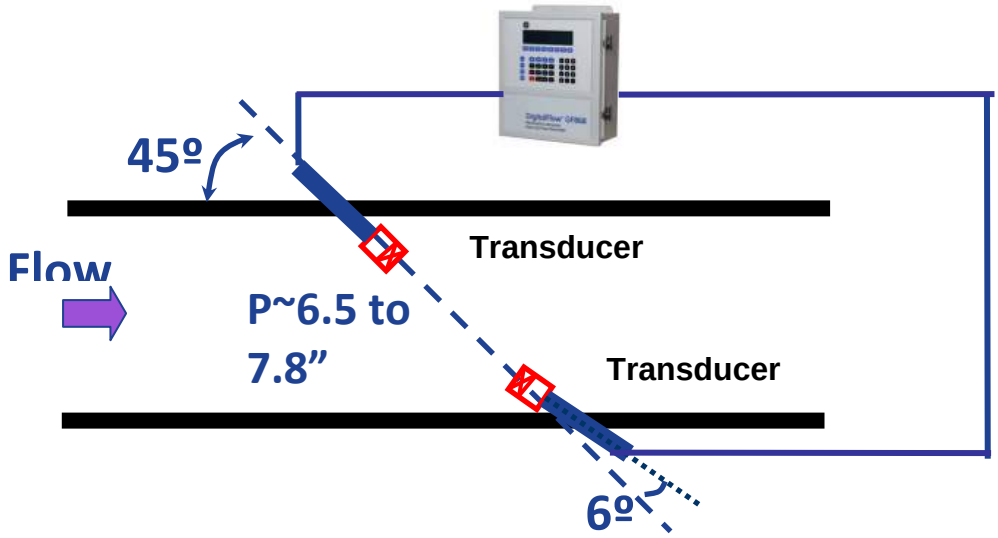

Figure 4. Conceptual design of the flare gas ultrasonic flowmeter.

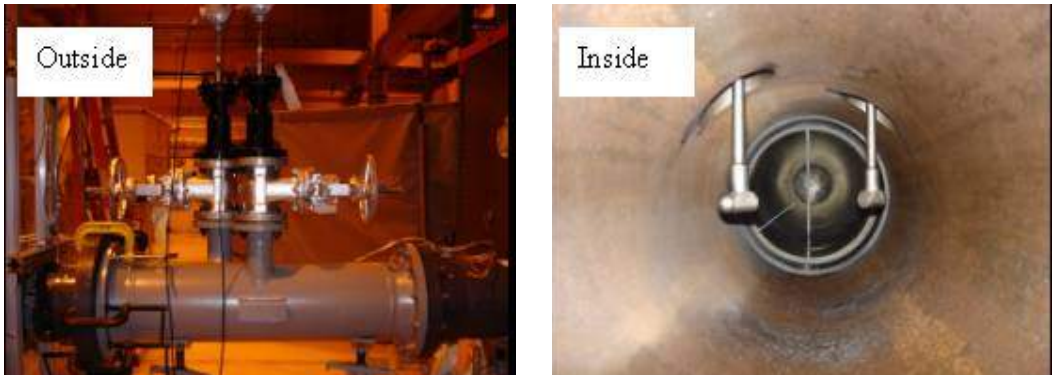

Figure 5 (a). Pictures of the Bias 90 carbon steel flowcell with transducers mounted, outside and inside views.

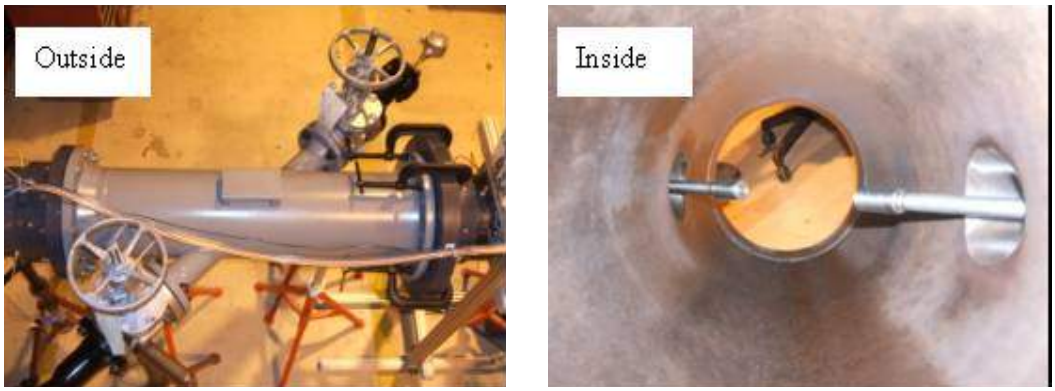

Figure 5 (b). Pictures of the Diagonal 45 carbon steel flowcell with transducers mounted, outside and inside views.

2.5 Testing Facility

Flow testing was performed in the Energy and Propulsion Technologies Laboratory at the GE Global Research Center (GRC) located in Niskayuna, NY in November 2008. Fig.6 shows the overall layout of the testing facility. Air was supplied by an open circuit high mass flow system, which consists of a three stage centrifugal blower, capable of 0 to 20,000 scfm, with 16-inch piping and multiple control valves. An inline Venturi tube was utilized to measure the flow. The 16-inch piping gradually expands into a plenum, upon which the test apparatus is attached. Perforated screens inside the expansion and plenum ensure uniform flow.

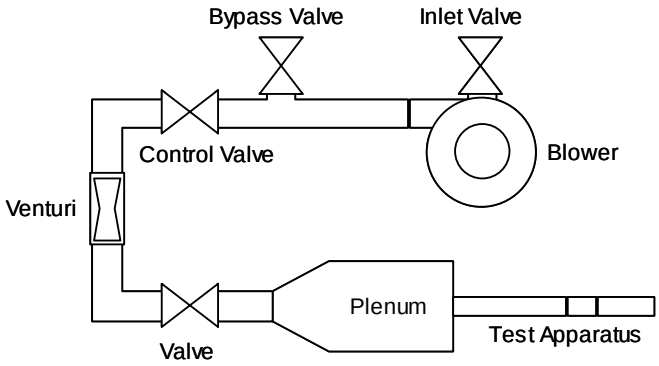

Figure 6. Illustration of open flow system at GE GRC.

2.6 Test Results

Fig. 7 shows the flow readings from the meter (called GF868) in comparison with the GRC reference readings, for the Bias 90 configuration and the Diagonal 45 configuration, respectively. As seen our meter readings agree with the reference readings very well across the velocity range of 31.2 m/s up to 123.7 m/s.

The percentage errors for both Bias 90 and Diagonal 45 configurations are within 2% across the velocity range of 31.2 m/s up to 123.7 m/s. With the reference accuracy of 1-2% (dependent upon the flow velocity range, refer to Appendix for details), we can conclude that the overall meter accuracy is better than 3-4%.

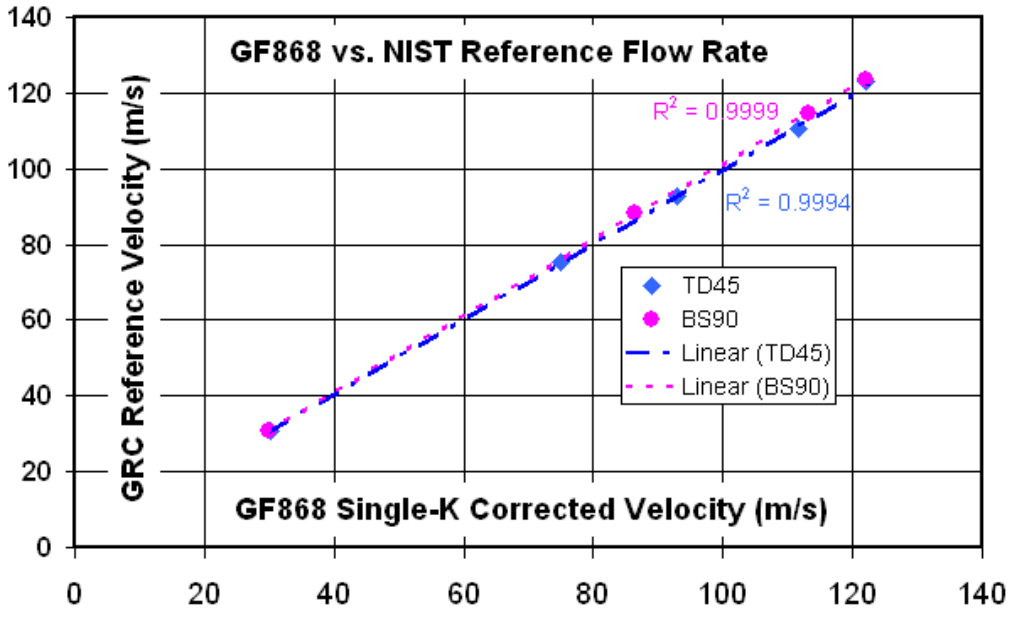

Figure 7. Flare meter reading in comparison with GRC reference reading for the Bias 90 configuration (BS90) and the Diagonal 45 configuration (TD45).

3 HIGH CO2 CONTENT FLOW MEASUREMENT

The flow rate of Flare Gas with a high concentration of Carbon Dioxide is becoming an important measurement for the petrochemical industry. In fact very new legislation for monitoring of Green House Gases has been issued by the EPA in the USA under 40CFR *Mandatory Reporting of Greenhouse Gases (GHG); Final Rule.* Flare gas monitoring for calculating CO2 emissions is mandated under Part 98 and covers petrochemical facilities. The EU has had directives for reporting of GHG for sometime now

3.1 CO2 Attenuation

CO2 is known to have an attenuating effect on ultrasound, and this can add to the already challenging flow measurement of flare gas with an ultrasonic flowmeter. The attenuation of CO2 has been known for quite some time and is comprised of two main components. There is classical attenuation simply due to density and distance between transmitter and receiver, and then there is the Relaxation effect due to the nature of the CO2 molecule. The primary illustration of these attenuation effects is seen in the chart below [16], see fig. 8.

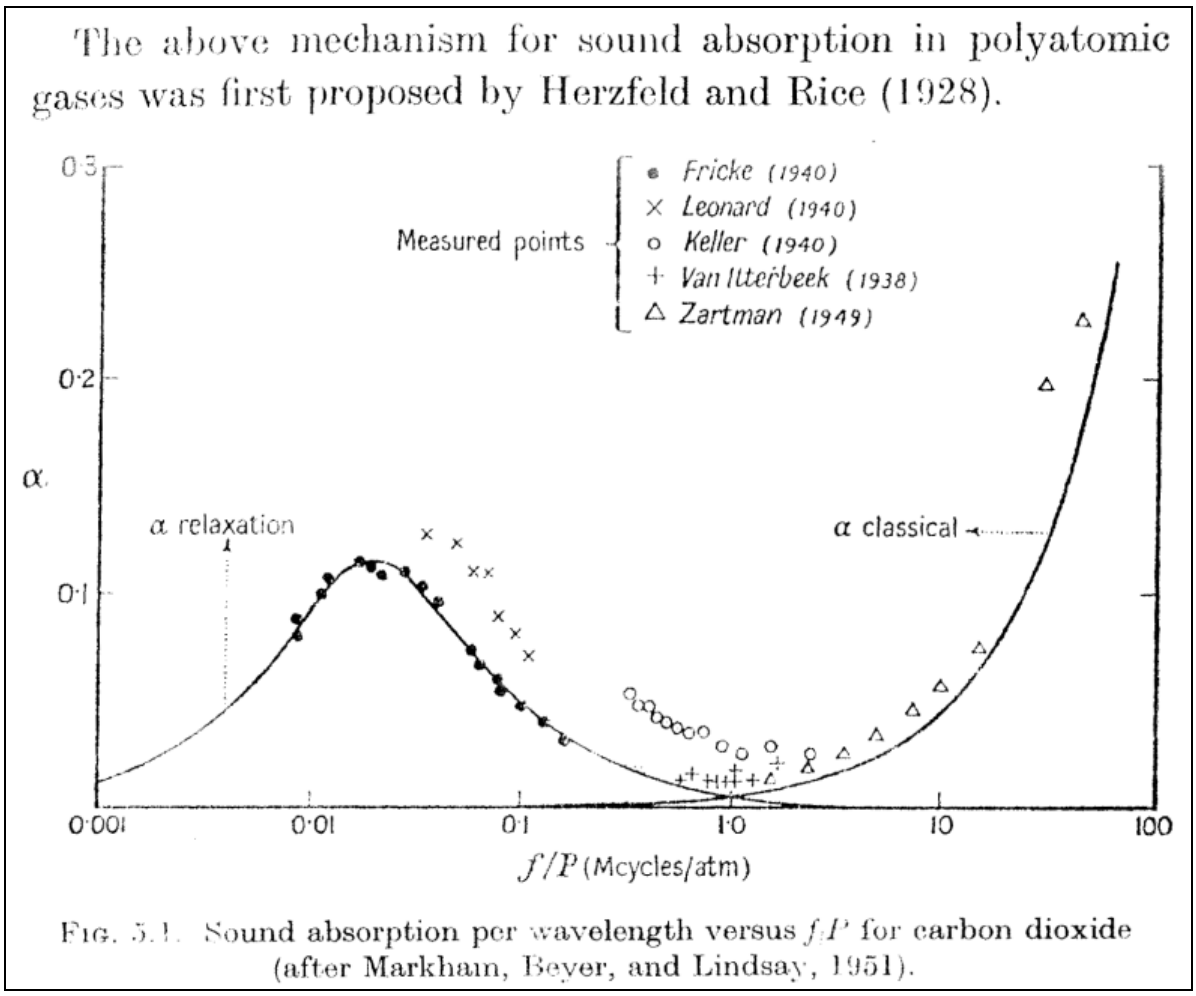

Fig. 8 Classic and Relaxation Effect attenuation in CO2 from [16]. Note Relaxation is directly proportional to frequency, yet inversely proportional to pressure

Original testing by us (Panametrics) was done with the then Exxon Co. back in the early 1980's in Baytown, Texas as part of the development of the Flare Gas Flowmeter. Shown here is a set of data collected from various gases including CO2 and other flare gases from 1982.
This testing as well as implementation of the Flare Gas flowmeter into working flare lines showed that while CO2 gas was attenuating, it was not overly difficult to still make flow measurements.

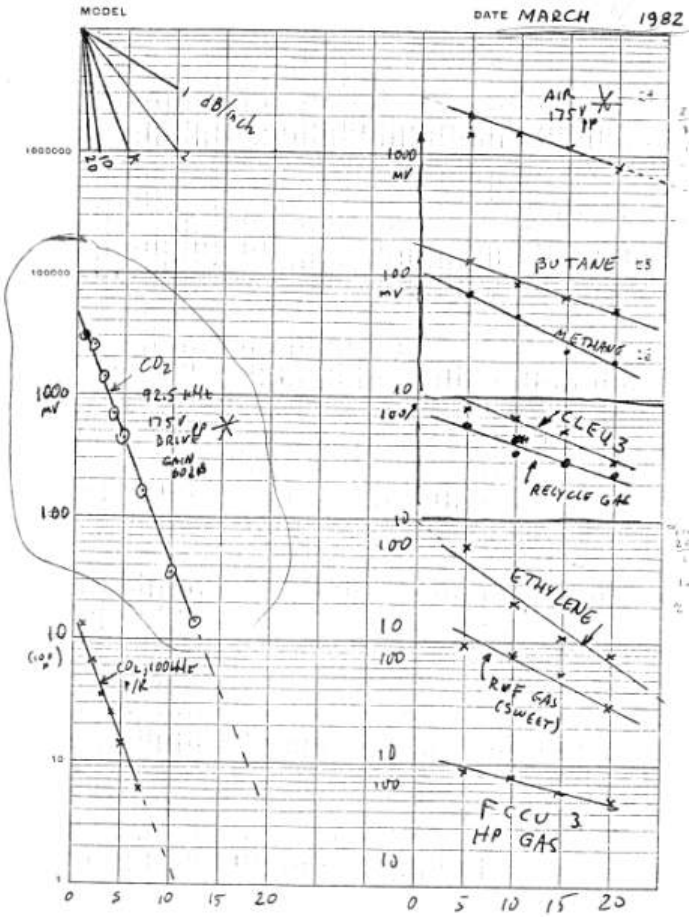

Fig. 9 Original plot of different flare gases' attenuation

Test	Test results		
MOLECULAR WEIGHT MEASUREMENT			
gas/gas mixture	True M.wt g/mole	Output error, % reading display	current
100% methane	16.04	- 8.0	- 7.2
100% n-butane	58.12	+ 5.8	(note 1)
50% ethane, 50% nitrogen	29.04	- 5.9	- 5.6
50% ethane, 50% nitrogen	29.04	+ 4.2*	+ 4.8*
100% ethane	30.07	- 0.7	- 0.5
50% ethane, 50% carbon dioxide	37.04	- 5.6	- 5.2
85% ethane, 15% nitrogen	29.76	- 2.0	- 1.7
85% ethane, 15% nitrogen	29.76	+ 2.3*	+ 2.8*
85% ethane, 15% carbon dioxide	32.16	- 2.0	- 1.6
98% ethane, 2% carbon dioxide	30.35	- 0.8	- 0.5
98% ethane, 2% nitrogen	30.03	- 0.8	- 0.4
98% ethane, 2% nitrogen	30.03	- 0.2*	+ 0.2*
50% methane, 50% n-butane	37.08	+ 2.2	+ 2.6
	note 1: no result given as the output was out of range and limiting.		

Additional testing by an independent organization, SIREP, was conducted in 1995. The data here shows the performance of the Flare gas flowmeter with varying compositions, many with a high CO2 content.

Fig. 10 Independent testing of an early flare gas flowmeter included CO2 mixtures.

3.2 Solutions

An in-house laboratory study of the CO2 attenuation effect was conducted in 2005 to model the effects on ultrasound. The volume fraction of CO2 in N_2 was modelled.

Model

Assume a measurement model as shown in Figure 11 where one transmitting transducer transmits acoustic waves into acoustic medium (here a mixture of CO_2 and N_2) and one receiving transducer receives those waves.

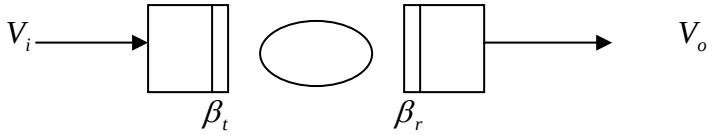

Figure 11. Measurement model

The receiving voltage from the measurement model can be written as

$$V_o = V_i \beta_t C A \beta_r \tag{7}$$

where

V_o is the output voltage

V_i is the input voltage

β_t is the transmission efficiency factor

C is the diffraction coefficient (reflecting beam spreading effect)

A is the attenuation of the medium

β_r is the receiving efficiency factor

The model uses transducers that are 100kHz type. We fix transducer size, distance, temperature, and pressure. Then physically if we only consider the terms that are possibly associated with gas components we have

$\beta_t \propto \rho c$ (proportional to acoustic impedance of medium)

$C \propto \frac{ka^2}{D} \propto \frac{1}{cD}$ (proportional to the inverse of distance)

$A \propto e^{-\alpha D}$ (attenuation in the exponential form)

$\beta_r \cong \text{constant}$ (transmission through a rigid body)

where

c is the sound speed in the gas mixture

D is the distance between the two transducers

α is the attenuation factor

Here we only focus on the attenuation change versus fraction change of CO_2 in N_2. Combining the above four terms yields

$$V_o / V_i \propto \rho e^{-\alpha D} \tag{8}$$

For our very specific problem, from the above equation, we can see that the signal strength is only associated with the density and attenuation factor of the gas mixture.

Density consideration

For a mixture of CO_2 and N_2, assume the fraction of CO_2 is *F*. Then the density of the mixture is expressed as

$$\rho = \rho_{CO_2} * F + \rho_{N_2} * (1 - F) \tag{9}$$

where ρ_{CO_2} is the density of CO_2 and ρ_{N_2} is the density of N_2.

Attenuation consideration

The attenuation factor is non-dimensionalized by the wavelength, or $\alpha\lambda$ is given instead of α itself. Then we need to consider the following expression,

$$\alpha = (\alpha\lambda)\frac{1}{\lambda} = (\alpha\lambda)\frac{f}{c} \tag{10}$$

where *f* is the frequency (=100kHz here). The sound speed is written as

$$c = \sqrt{\frac{\gamma RT}{M}} \tag{11}$$

where

$\gamma = \frac{C_p}{C_V}$ is the adiabatic constant

T is temperature in Kelvin (here we take *T*=298.15K)
R = 8.314 J/mol/K
M is the molecular weight of gas

By considering the fraction of CO_2 in the mixture, we have

$$\gamma = F * \gamma_{CO_2} + (1 - F) * \gamma_{N_2} \tag{12}$$

and the molecular weight

$$M = F * M_{CO_2} + (1 - F) * M_{N_2} \tag{13}$$

Via Eqs. (11), (12) and (13), we see that attenuation is a function of the fraction of CO_2 in N_2.

Simulation

From [13], the attenuation of CO_2 in N_2 was measured from 20% to 80% and is shown in Figure 12. This figure shows the dimensionless $\alpha\lambda$ versus frequency divided by pressure. This is called the attenuation spectrum.

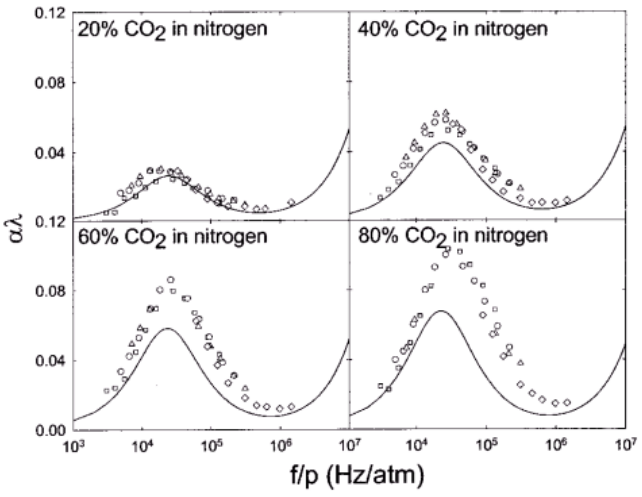

FIG. 10. Results for mixtures of 20%, 40%, 60%, and 80% CO_2 in nitrogen with the Pinkerton diffraction correction at average temperatures of 292.6, 293.7, 293.5, and 294.0 K, respectively. Data points are for the 92 kHz, 149.1 kHz, 215 kHz, and 1 MHz transducers (squares, circles, triangles, and diamonds, respectively). The solid curves are the calculations based on the vibrational relaxation model of Dain and Lueptow (Ref. 3) summed with the classical and diffusional attenuation.

Figure 12. Attenuation with CO2 in N2 from [17].

Here we only consider the case where *p*=1atm and thus the X-axis is the frequency. Extracting the values of $\alpha\lambda$ at 100kHz (10^5) in the four subplots we then fill them into the following table.

Table 1 - Measured data at 100kHz and 1atm

Fraction of CO_2 in N_2	Attenuation ($\alpha\lambda$)
20%	0.0125
40%	0.036
60%	0.052
80%	0.08

In the table, we only have four data points. Using linear fit, we obtain

$$(\alpha\lambda) = 0.10925 * F - 0.0095 \quad (14)$$

This equation is only valid from 20% to 80% of CO_2 in N_2. Then Eq. (8) is rewritten as

$$V_o / V_i \propto \rho e^{-(\alpha\lambda)\frac{Df}{c}} \quad (15)$$

Substituting Eqs. (9), (11) and (14) into Eq. (15) gives the relationship of the signal strength to the fraction of CO_2 in N_2.

Figure 13(a) illustrates the signal strength change with the fraction of CO_2 in N_2. This change only has relative significance. Figure 13(b) illustrates the linear trend of the signal strength in terms of dB with respect to the strength at 20%. From Figure 13(b) we could see that the signal strength is reduced by about 7.2dB when the CO2 is increased by 10%.

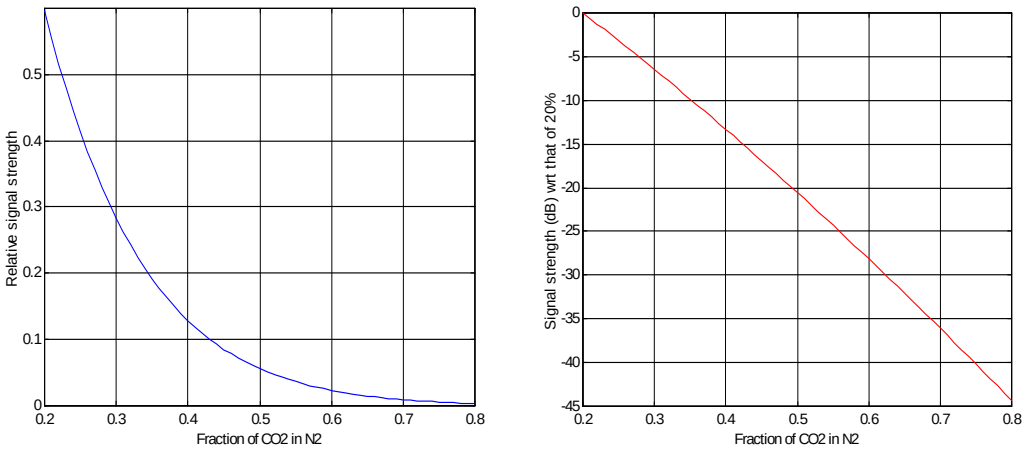

(a) (b)

Figure 13. Simulation

Transducer

To help avoid the highest attenuation from the Relaxation effect, and even from classical attenuation. The flare gas flowmeter can use a variety of ultrasonic frequencies for the transducer. The most common frequency is 100 kHz as used in the model above. The next lower frequency is 50 kHz, and because of its longer wavelength it is also a larger transducer. On some occasions higher frequencies are called for with 200 kHz being common, and 500 kHz rare, but possible. One major feature that differentiates one transducer from another is the power of the transducer designed and used. A more powerful transducer can overcome these forms of attenuation even at non-optimum frequencies.

Fig. 14 A variety of ultrasonic transducers, at different frequencies, are used in flare gas flow measurement.

3.3 Performance Test

In 2009 through 2010 we conducted testing for performance or accuracy impact from CO2 content in gas compositions. [19] Testing was done with the CTF878 gas clamp-on flowmeter, which has the following specifications:
Velocity Accuracy: 2% of reading
Repeatability: 0.6% of reading
Range ability: >100:1
Gas pressure: tested from ambient to 100bar
Gas temperature: tested from subzero to 450^{O}F
Pipe size: ϕ 2" to ϕ 30"
Turbulent flow only.
The CFT878 uses ultrasound to make flow measurement in steel pipes using the Tag Correlation method at frequencies of 200 to 500 kHz.

A baseline performance test was done on the same high velocity air flow loop at GRC in 2009 shown in fig. 15.

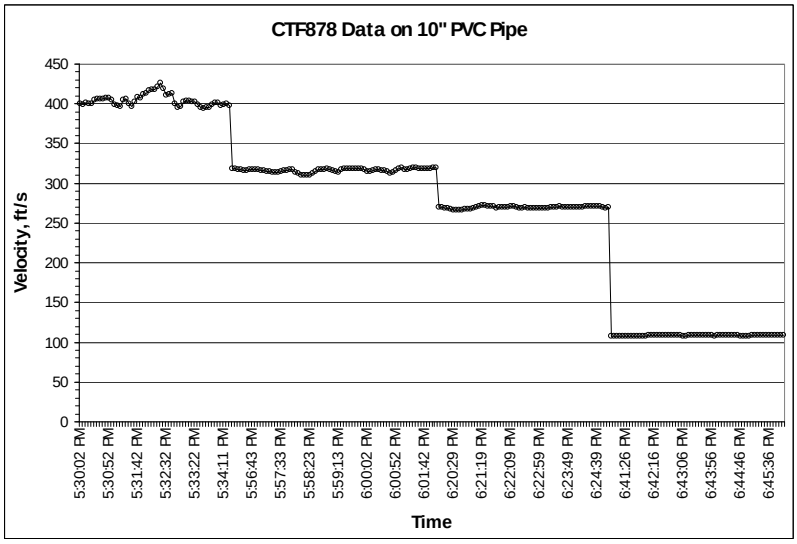

Fig. 15 CTF878 on 10" PVC pipe tested over full velocity range at GRC

The accuracy of the flow meter against the reference flow is plotted below in fig. 16.

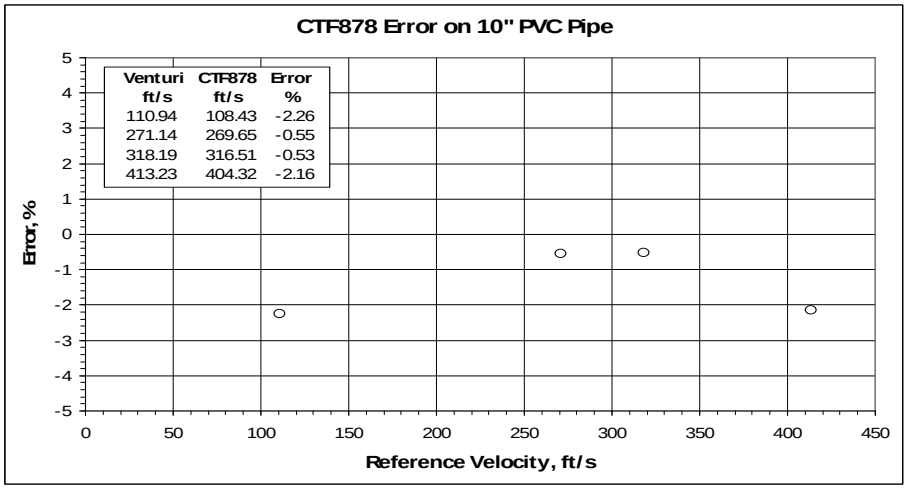

Fig. 16. Accuracy plot of clamp-on flowmeter velocity vs. the GRC reference.

The clamp-on meter was then compared to a reference flowmeter at a flow loop at the author's laboratory using various mixtures of CO2 with air. See fig 17 below for flow loop illustration.

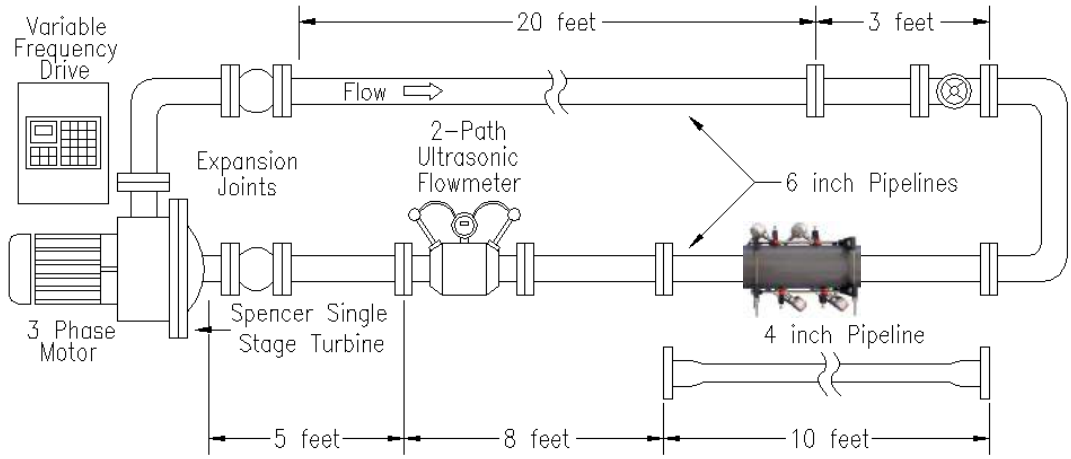

Fig 17 Compressed air loop, gas pressure up to 100psig and velocity up to ~120ft/s with CO2 mixtures.

As shown in fig 18 below, the relative accuracy of the flowmeter is unchanged for the various mixtures of CO2 with air, even at different pressures. No additional error is introduced with up to 30% CO2 within the meter specification Influence of CO2 on flow measurement in larger pipes (>12") or at higher pressure is expected to be even smaller when lower frequency transducers are applied.

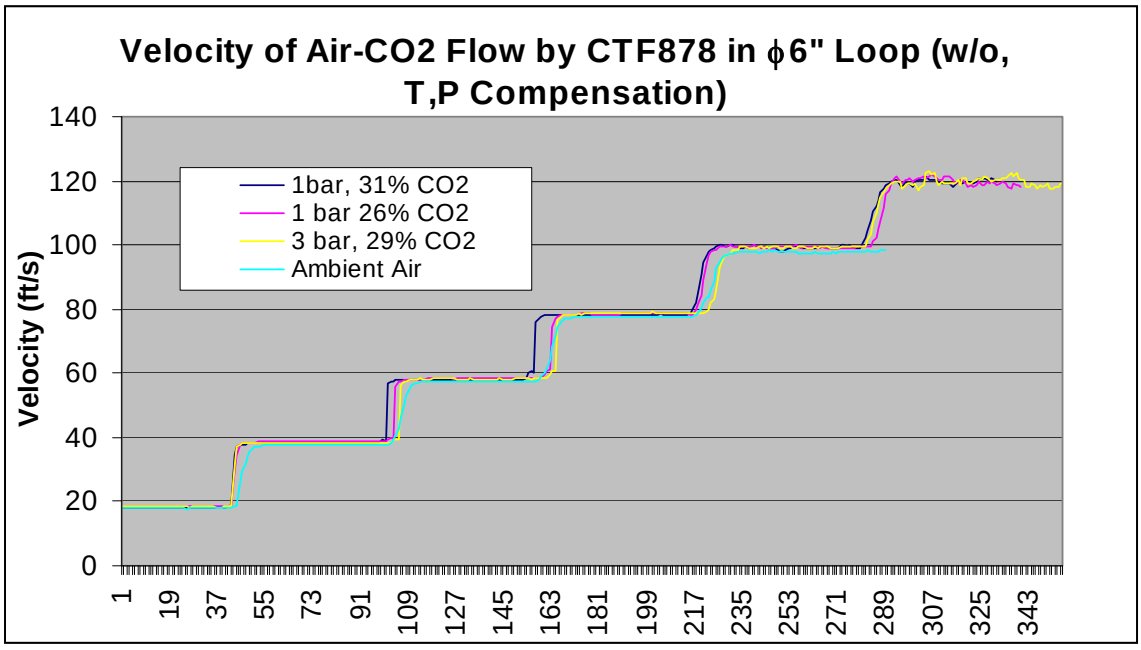

Fig 18. Accuracy of flow measurement is unchanged for various mixtures of CO2 with air at various pressures.

3.4 Application Review

To have a successful application with an ultrasonic flowmeter in gas streams with CO2 content it is required to review the conditions of the application to see if the ultrasonic frequency is right and to adjust the path length if necessary. Plotted below are some actual applications at different pressures, and other process parameters. The data put together here show that by avoiding the peak attenuation of the Relaxation effect the Ultrasonic Gas Flow Meter is quite capable and reliable over a wide variety of CO2 content, pipe size and pressure, see Table 2.

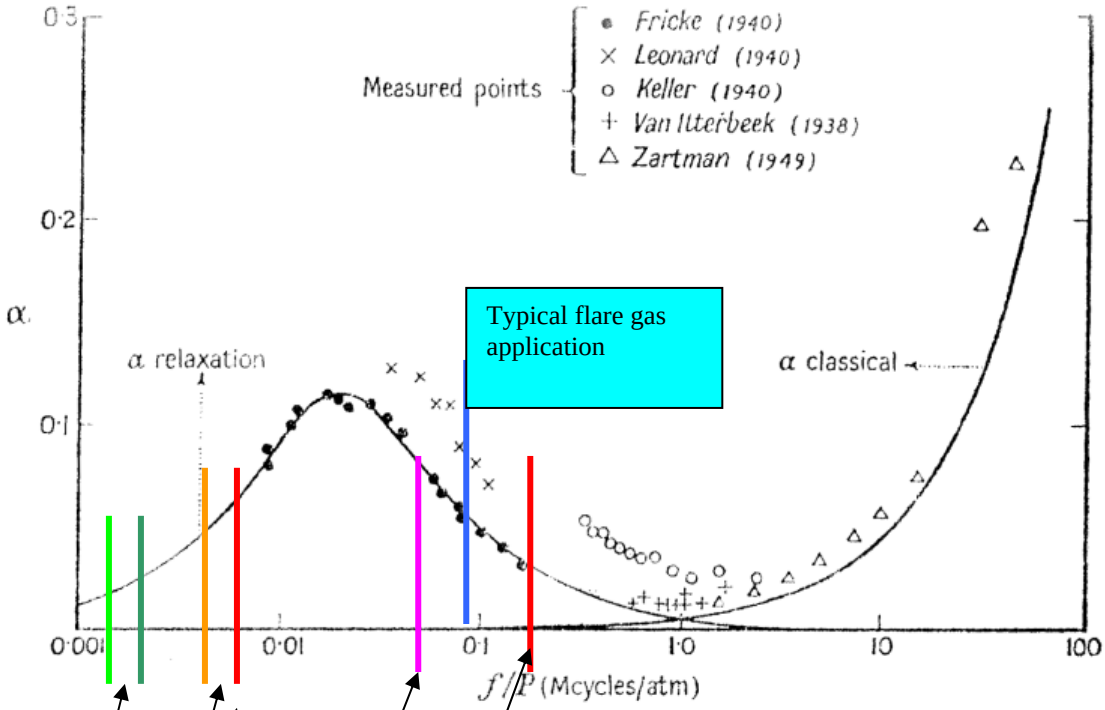

Fig. 5.1. Sound absorption per wavelength versus f/P for carbon dioxide (after Markham, Beyer, and Lindsay, 1951).

Application	Press (barg)	Press (atm)	Temp. (degree C)	CO_2 mole%	Mcycles/atm
XGM with 200 kHz BWT	1.39	1.372	185	78.5-90	0.146
XGM with T14	1.59	1.57	65	78.5-90	0.063

Application	Min Press (barg)	Max Press (barg)	Temp. (degree C)	Pipe Size (Meter Size)	Flow Rate (MMSCMD)	CO_2 mole%	Mcycles/atm (100 kHz)/ min P	Mcycles/atm (100 kHz)/ max P
AI	15	20	22.28	DN450	4.543	20%+	0.0067	0.005
B,C,D	40	60	22.61	DN400	3.936	20%+	0.0025	0.00167
E,F	15	20	30.01	DN250	1.343	20%+	0.0067	0.005

Fig. 19 Some actual field applications plotted on the attenuation curves at 100 kHz.

Table 2 - Process Applications with CO2

Application	Natural Gas Transport	Process	Process	Process	Coke Oven Gas (COG)	COG	COG	Steel (LDG)	Flue Stack	Process BFG (Flue)	Blast Furnace Gas	Flare	Flare-CO2 Recovery Injection	Flare
Qty/Size	9	24"	1 x 14"	1 x 400mm	1	1 x 40"	1 x 40"	1 x 1829 mm	6.34 meter	1	1 x 40"	1 x 24"	3 x 12-24"	1 x 36"
Location	Kazakhstan	Wyoming, USA	California, USA	East Europe	Asia	Japan	Japan	Japan	Spain	Asia	Japan	Texas, USA	Texas, USA	Wyoming, USA
User	IHC/SBM	ExxonMobil	Exxon	----	----	----	----	----	----	----	----	----	Oil co.	Amoco
Install date	2005	2004	2003	<2009	2007	<2008	2008/2009	2009	2005	2007	2008	2008	~1995	1994
Pressure	28 bar	(600#)	2.04 bar	1.08 bar	1.039 bar	1.045 bar	1.196 bar	1 bar	1 bar	1.078 bar	1.062 bar	1.55 bar	1-1.3 bar	1 bar
Composition														
Methane	51.076	1.5			26.6		29.2					1.4		
Nitrogen	0.562	3		48	2.3		3.4	18.1	71.8	54.1				
Ethane	10.785						2.3					0.82		
Propane	5.335											0.62		
Iso-butane	0.765													
N-butane	1.511													
Iso-Pentane	0.401													
N-pentane	0.394													
CO2	**5.649**	**69**	**100**	**7**	**3.1**	**2**	**2.1**	**16.4**	**14.2**	**20.7**	**23**	**97.16**	**85-90**	**>95**
CO				22	8.4		6.1	64.6		22				
H2S	22.076													
Hydrogen		12		18	56.4		56.4	0.9		3.2				
Hexane														
C6+	0.65													
H2O	0.796			5					10.88					
Other		14.5			2.9	98	0.5				77		15-Oct	<5
Oxygen					0.3				3.12					

Fig. 20 This installation is on a 14 inch pipe, with a 19 inch path. In 100% pure CO2. Temperature is ambient and pressure approximately 30 PSIA. Plot of freq/pressure =0.05 with a 100 kHz transducer is shown.

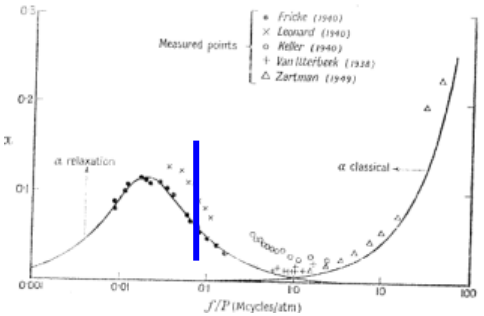

4 LOW VELOCITY FLOW

Regulations on emissions in North America, Europe, and even Asia, around Green House Gases and other materials have made petrochemical facilities with Flares look closely at low flow velocities. Users and Regulators are realizing that continuous low flow can add up to significant quantities of gas. Stack emissions allocations can be reached with low flow, and not just with relief flow rates.
The low flow regime is typically from 0.03 to 0.3 meter/second (0.1 to 1 feet/second) in terms of velocity.
Current accuracy requirements at these low flow velocities is not always well defined by regulations, but is typically given as +/-20% at and below 0.3 m/s. However the trend is for better: to 5%.
In some regions the flare stack is given, or allocated, a total amount emissions it can produce in a time interval, typically a year. More accurate measurement of this low flow will allow users to operate longer before these allocation limits are exceeded.

4.1 Two Part Challenge

The flow velocity in flares is often in the range below 0.3m/s, but it is important that we look towards ways of improving the measurement accuracy over that range of velocities but still make a measurement at the high end of the velocity range during facility relief or upsets. Low flow presents two major challenges for the flow meter. Firstly is the resolution in velocity measurement by the meter itself, and secondly the asymmetric flow in the pipe where non-axial flow is on the same magnitude as axial flow.

4.1.1 Accuracy/Resolution at Low Flow

In the transit time ultrasonic flowmeter the measurement of time and distance determines the fundamental resolution in velocity. For the current meter the time measurement resolution is on the order of 50 nanoseconds (nS) at higher flow rates, and about 10 nS for lower flow rates. (The noise (SNR) at high flow limits the resolution).
The typical path length, or distance, is based on the installed transducer configuration. It is the projection of that path (L) in flowing fluid that directly affects velocity. The gas composition now enters the calculation since that determines the sound speed, and we use the following approximation to determine resolution in velocity:

$$V = \frac{\Delta t \bullet c^{2}}{2L} \qquad [16]$$

where

V_o is gas flowing velocity

Δt is resolution in time of the difference in transit times

L is axial projection of the path length in flowing fluid

c is the sound speed of the gas

For the Bias 90 configuration the most common path length is about 1.08 feet or 0.329 meter with an L of 0.233 meter. A common flare gas sound speed might be 410 m/s, and using 50 nS for time resolution we get a velocity resolution of 0.018 m/s. At a flow rate of .3 m/s this is about 6% inaccuracy, and at .03 m/s about 60% inaccuracy. However at low flow the meter will use the 10 nS resolution and the associated velocity resolution will be .0036 m/s. At 0.3 m/s this will calculate as inaccuracy of ~1.2%, and at 0.03m/s the inaccuracy shows as about 12%.
Actual inaccuracy will change if the gas composition produces a different sound speed, with higher sound speeds (i.e. hydrogen) increasing the inaccuracy.

For the Diagonal 45 configuration the same calculations hold true. As above the inaccuracy will depend on the path length, with longer paths lengths (an longer L) giving smaller values for velocity resolution and hence lower inaccuracy.
However there is a limit to how long a path can be since the attenuation of the ultrasonic signal is a function of the distance between transducers, as shown in section 3.2 above.

4.1.2 Asymmetric Flow

The second challenge of low flow is asymmetric, or non-axial flow velocity contributing to a significant degree to the transit times. The non-axial component of flow measurement is an error in the average flow measurement, unless it can be accounted for or eliminated.
Non-axial flow takes the form of cross flow or circulation. This can be induced by convection flow within the piping, or by stratification of different density gases within the total gas composition.

Convection generated cross or circulation flow may dominate over axial flow in magnitude at very low flow rates. A single path measurement may not be sufficient to eliminate or reduce this error. To illustrate this consider the following case of a large flare gas main header pipe at a Texas, USA facility. This flare line was instrumented with both a Bias 90 and a Diagonal 45 path configuration as shown in the figure 21 below:

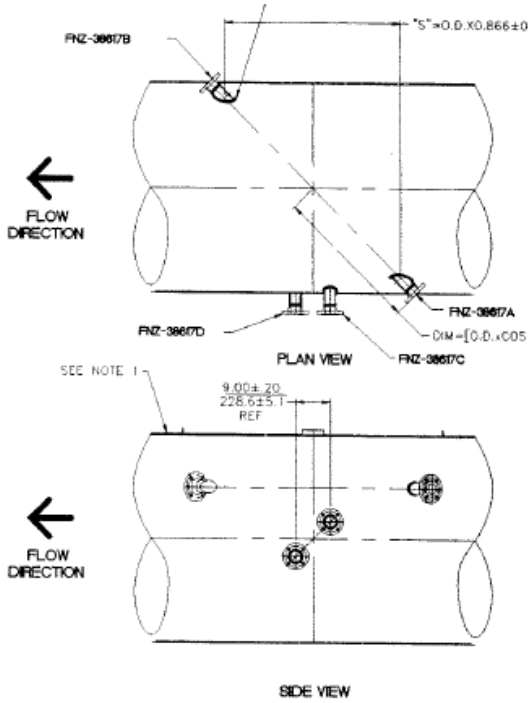

Fig. 21 Here we see two views of the transducer ports on this pipe. The Bias 90 set are close together, while the diagonal 45 set are virtually on opposite sides of the pipe. The diagonal 45 configuration is not on the diameter, but is an off-diameter path.

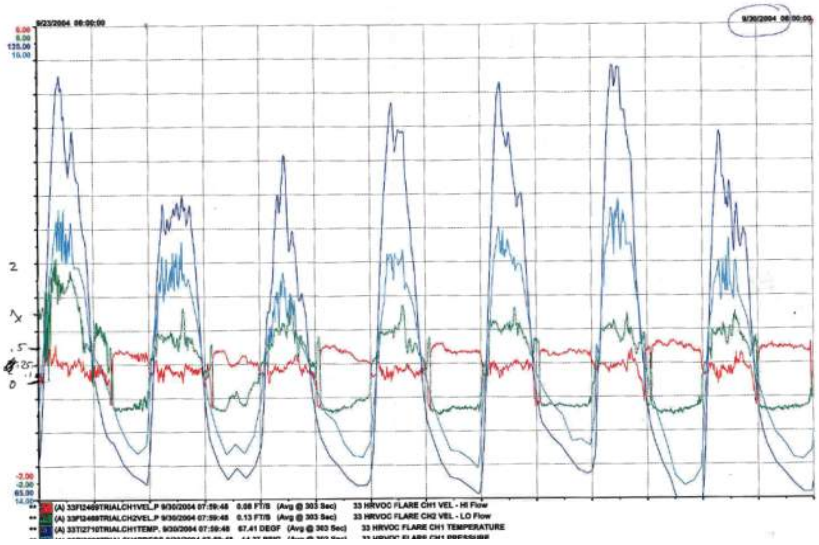

Fig. 22 Control room plot of the Bias 90 and Diagonal 45 flow rates along with pipe temperature and pressure. Showing the flow rate changes about 0.15 m/s on the bias 90, and from +0.3 to –0.3 m/s on the Diagonal 45 twice a day at about 8 am and 8 pm.

This behaviour can be explained by convection flow changing the direction of cross flow. As illustrated in the figure below it only takes a very small change in the direction of the cross flow to make the Diagonal 45 path appear as if the flow reversed direction, when in fact it did not. The Bias 90 path is not sensitive to this direction of cross flow, so it measures the axial flow alone.

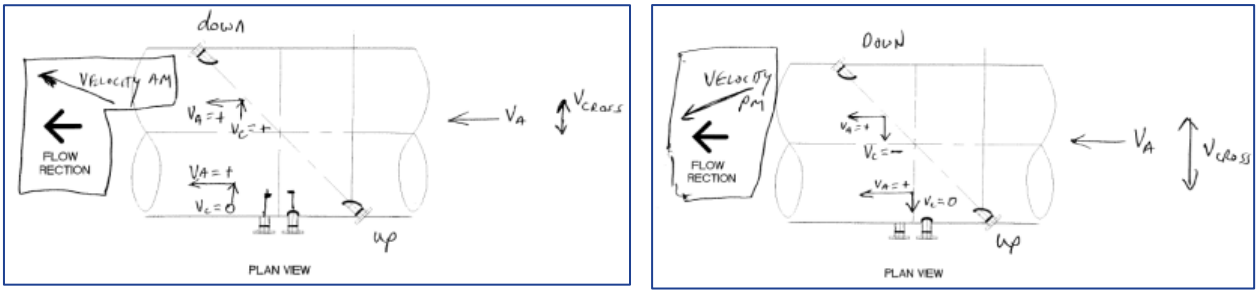

Fig 23 Schematic representation of the axial flow, Va, the cross flow, Vc and how a slight change in the cross flow direction can reverse the flow indication on the Diagonal 45 path, but not the Bias 90 path.

To verify the idea that convection flow can show these low flow effects, the ambient temperature of the city where the flow meter is located is plotted against the trend flow rate data for the same dates. In this case the match in unmistakable. See fig 24.

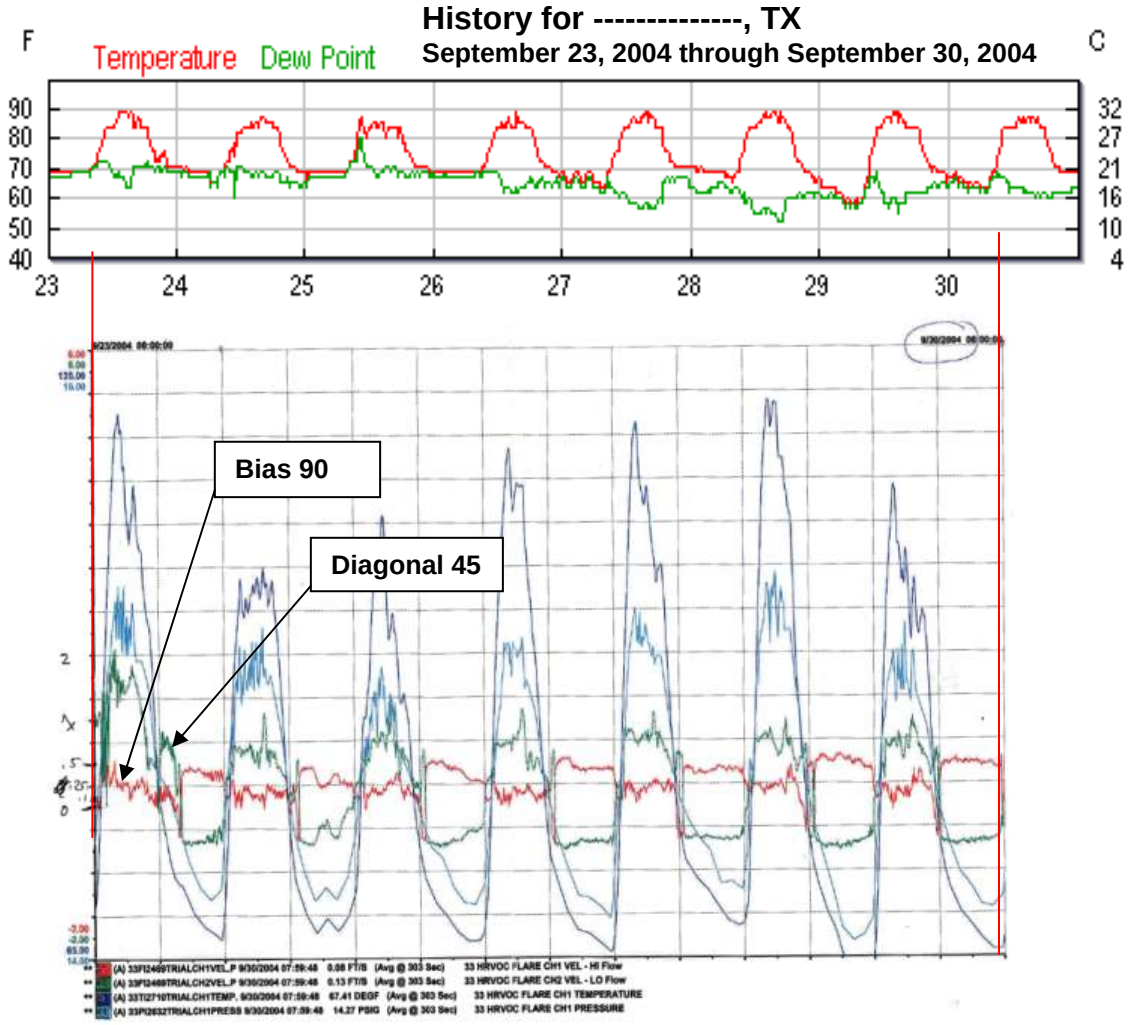

Fig 24 The historical temperature data for the location of the facility where the meter is located plotted against the observed flow rates form the two paths.

Convection flow as well as stratification is also exhibited on this 24" flare line where the meter is showing low flow peaks that also follow the ambient temperature. With up to 70% Hydrogen, by volume, possible in the pipeline, circulation flow seems to be present at the lowest flow rates where the different density gases can separate.

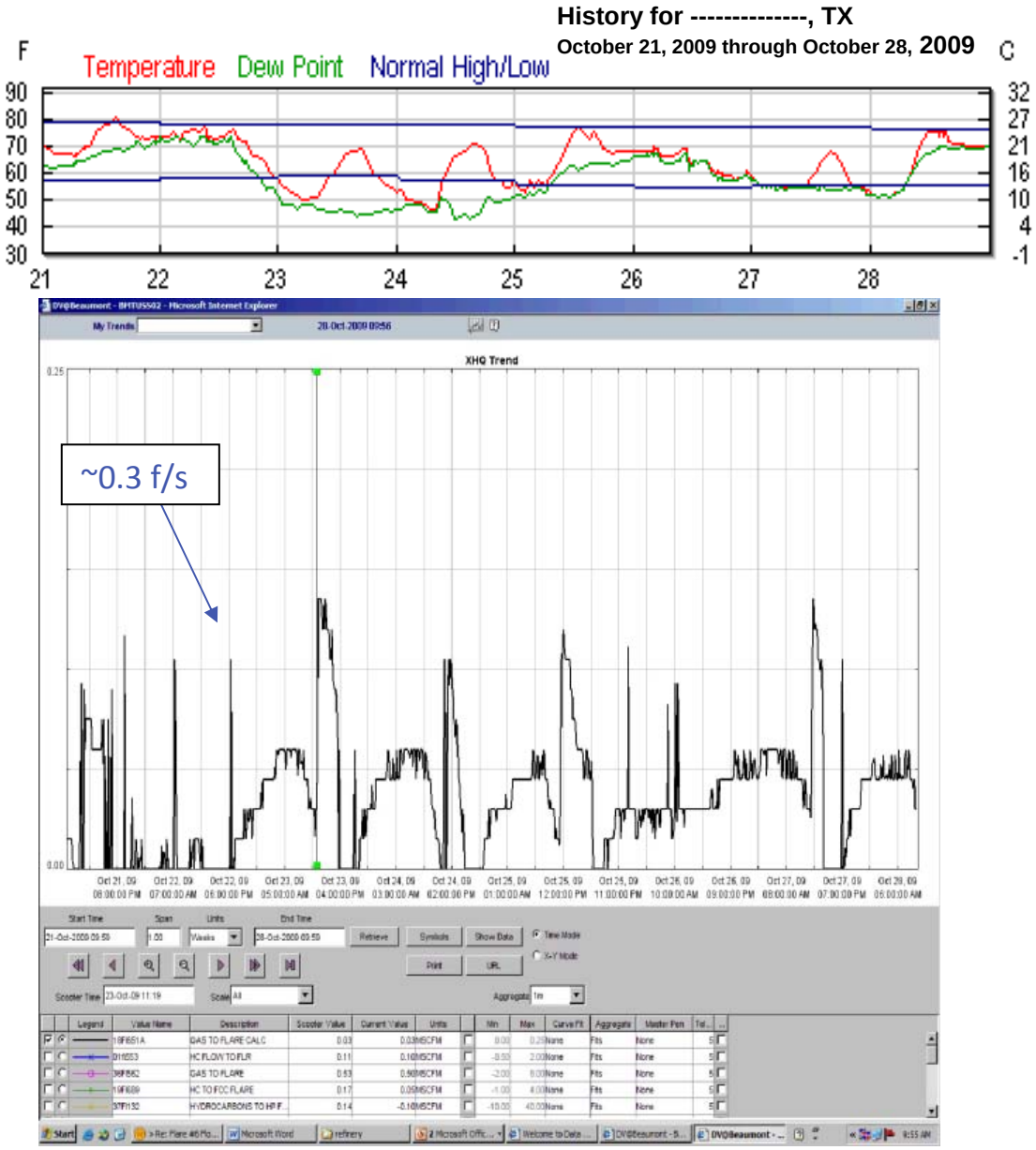

Fig 25 A 24" flare with a Bias 90 installation on the top of the pipe. Stratification and convection flow producing peaks of low flow based on the ambient temperature, but not evident at the flare tip.

4.1.3 Convection Model in CFD

To help verify the convection flow in the flare line we have applied CFD (Computerized Fluid Dynamics) to a model of convection flow. Fig. 26 shows the convection flow induced by a 20 C differential between top and bottom (or any opposite sides) of a circular pipe. Note flow rates from 0.09 to 0.3 m/s.

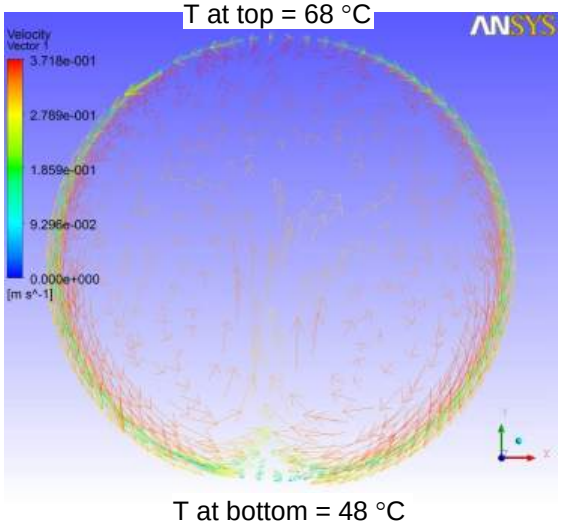

Fig 26 Convection flow of gas in a 24" pipe with 20 C temperature difference top to bottom.

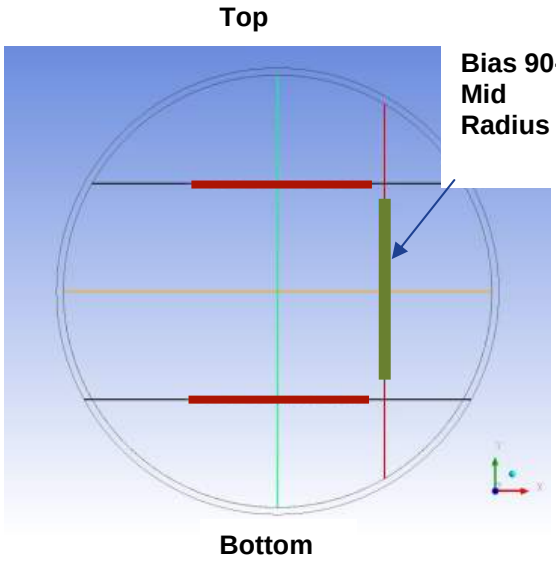

Fig 27 Diameter, Mid-Radius and bias 90 paths are modelled.

The results have demonstrated that the natural convection due to the temperature gradient from solar radiation is significant. [18]
Cross flow can be 8 to 15% of a 0.3 m/s (1 f/s) mean flow rate (Vm) at these very low velocities. It depends on path position, the actual mean flow velocity and the solar radiation absorption of the system.

	up/Vm	vp/Vm	wp/Vm	Vpath	k=Vm/Vpath
Dia X A	0.00047	0.00278	0.98401	0.29928	1.01577
Dia X B	0.00093	0.00126	0.98284	0.29850	1.01843
Dia Y A	-0.00019	0.15497	0.91371	0.32488	0.93574
Dia Y B	0.00026	0.15282	0.90984	0.23014	1.32096
Mid XR Y A	0.00108	-0.02912	1.04361	0.30840	0.98572
Mid XR Y B	-0.00029	-0.02698	1.04410	0.32561	0.93364
Mid YR X A	-0.00197	0.01076	1.11274	0.33767	0.90028
Mid YR X B	-0.00160	0.00739	1.11556	0.33962	0.89513
Mid negYR X A	-0.00251	0.00196	0.97434	0.29544	1.02899
Mid negYR X B	-0.00388	0.00515	0.97286	0.29693	1.02382
Mid XR Y A Bias	0.08211	0.00196	0.97434	0.29544	1.02899
Mid XR Y B Bias	0.08080	0.00969	1.01771	0.30644	0.99204
Mid YR X A Bias	-0.00083	0.06433	1.10599	0.33597	0.90485
Mid YR X B Bias	-0.00038	0.06344	1.10836	0.33706	0.90193
Mid negYR X A Bia	-0.01039	0.21559	1.00426	0.30213	1.00617
Mid negYR X B Bia	-0.01094	0.21737	1.00290	0.30821	0.98635

Fig. 28 Average velocities along various paths with area averaged Vm=0.304 m/s. u and v are cross flow component, while w is axial flow component.

4.2 Low Flow Solutions

Solutions for accurate low velocity measurement in the flare line entail using different approaches, based on the individual conditions. For improved resolution the basic choice is one longer path. This may meet the requirement, but it can depend on gas composition, pipe size and how the asymmetrical flow is formed.
Two or more paths are now a common solution to get the highest accuracy over the widest range of conditions. In many cases the system will use one path for high flow and one path for low flow. Figure 29 below illustrates the addition of a Diagonal 45 diametrical path to the existing Bias 90 path on the 24" pipe shown above. The result is improved performance at the low flow showing a better average of asymmetric flow, while maintaining the performance and accuracy at high flow even with high amounts (to 70 %) of hydrogen.

Fig. 29 24" flare line now with both original Bias 90 installation and with diametrical Diagonal 45 installation

The Diagonal 45 path will have longer path length, and resulting axial length, and will be able to measure the velocity with a greater resolution than the Bias 90 with it's shorter path. The Diagonal 45 path may be across the diameter, or unconventionally, at an off diameter location. The nozzle, or ports, for the transducers must be located to cause little or no interference with each other. See the illustrations below for examples of this. Alternatively the use of two Bias 90 configurations may provide sufficient accuracy improvement while allowing installation on flare lines with restricted access.

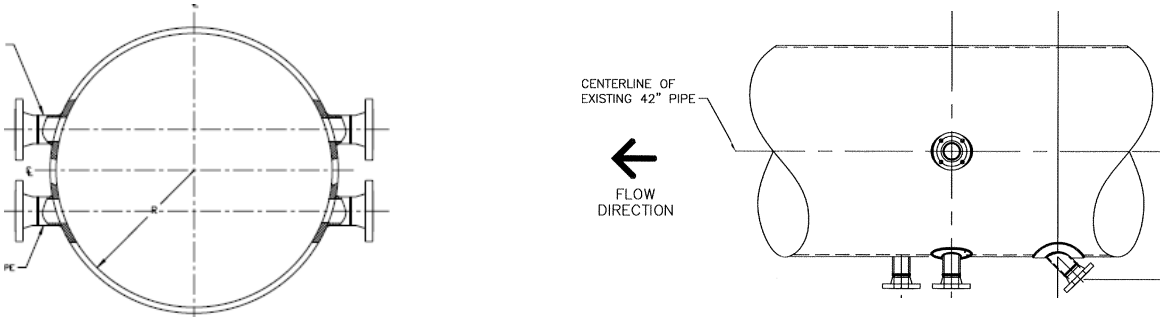

Fig 30 Left hand drawing shows two sets of ports for a two-path bias 90 installation. The right hand drawing shows Bias 90 ports with a second path in a "90-180" configuration. These systems can provide the accuracy required at low flow in difficult installations.

**Fig 31 Installed systems of two-path bias 90 (high flow) and a two-path Diagonal 45 (low flow).
Note separation of the two-path systems to avoid potential acoustic crosstalk**

5 CONCLUSION

In summary an ultrasonic flare gas flow meter has been developed to demonstrate the accurate measurement of air flow up to 123.7 m/s. Some of the new enabling technologies are detailed, primarily focused on the mechanical and transducer developments. Testing data have been presented for two typical configurations, Bias 90 and Diagonal 45, in comparison with a Venturi reference. The overall accuracy of the meter is shown to be better than 3-4% with reference meter uncertainty included, dependent upon the flow velocity range, and the relative standard deviation of our meter readings is within 1.2%. The new development could potentially translate into an even higher flow-velocity flare gas measurement, depending on the flare gas composition.
There is concern in the industry about the effects of CO2 on the ultrasonic flow meter's performance. While there is a specific effect due to the Relaxation effect of the CO2 molecule, it is dependant on parameters of frequency and pressure. This can be addressed with careful review of any application with appreciable CO2 content, and there have been many successful installations by selecting the proper transducer frequency and controlling the path length. The amount of CO2 mixed with other gases does not affect the accuracy of the volumetric flow rate measurement in the ultrasonic flowmeter.
Techniques of using longer path lengths, and two paths have been used to address the error seen at low flow, whether due to a need for improved resolution or to deal with asymmetric flow from convection flow or stratification.

6 APPENDIX: GRC REFERENCE UNCERTAINTY

All pressure and temperature measurements were made using National Institute of Standards and Technology (NIST) traceable instrumentation. At each velocity set point, a time delay preceded sampling to ensure flow stabilization. Each sensor would then be sampled for 10 seconds, at 10 measurements per second, and averaged for that point; this procedure was followed for all measurements. Each sensor was calibrated by NIST traceable calibration equipment prior to testing, in addition to manufacturer calibration. The uncertainty in the measurements varied by sensor type. For the static pressure sensors, the combined uncertainty, u_c, was +/–51.74 Pa, while the total pressure sensor u_c was +/–51.97 Pa. The Venturi measurement used pressure sensors with the upstream u_c equal to +/– 89.69 Pa and the throat u_c equal to +/–35.23 Pa. The temperature sensors used were standard type T thermocouples. The u_c values for the Venturi, stagnation chamber, and test section temperatures were +/–0.41 K, +/–0.42 K, and +/–0.41 K, respectively. The technique used to determine measurement uncertainty for the instrumentation is outlined in NIST Technical Note 1297 [15].
The u_c values were conservatively propagated through the velocity calculations for each measurement, and therefore varied at each velocity point. Typical velocity error for the profile measurements is less than 1.0%, with higher error values at the low velocities ($\leq$ 50 m/sec). Typical error for the reference velocity measurements is less than 2.0%, with higher error values at the low velocities ($\leq$ 50 m/sec). For example in uncertainty; the free stream velocity value of 120.6 m/sec +/–0.8 m/sec, and the reference velocity of 112.5 m/sec +/–1.8 m/sec.

7 REFERENCES

[1] J.W. Smalling, L.D. Braswell, L.C. Lynnworth, and D.R. Wallace, Flare Gas Ultrasonic Flow Meter, Proceedings from the Thirty-Ninth Annual Symposium on Instrumentation for the Process Industries, pp. 27-38,1984.

[2] D. Belock, How much do you flare?—How to measure flowrates of flare gas accurately and reliably, Process worldwide, Issue 3, pp. 18-19, 2006.

[3] NORWEGIAN PETROLEUM DIRECTORATE. Regulations to measurement of fuel and flare gas for calculation of CO2 tax in the petroleum activities, August 1993(ISBN 82-7257-395-4).

[4] L. Sui and T.H. Nguyen, Ultrasonic Flow Meter, US Patent Application No.12272174 filed in November, 2008

[5] K.S. Mylvaganam, High-rangeability ultrasonic gas flowmeter for monitoring flare gas, IEEE Transactions on Ultrasonics, Ferroelectrics and Frequency Control, Vol. 36, pp. 144-149, 1989.

[6] GE Sensing, GF868 Brochure, http://www.gesensing.com/downloads/datasheets/920_009c.pdf

[7] O. Rutten, Deutsches Patent No. 520484, 1928.

[8] L.C. Lynnworth, Ultrasonic Measurement for Process Control: Theory, Techniques, Applications, Academic Press, 1989.

[9] ANSI/ASME MFC-5M-1985, “Measurement of Liquid Flow in Closed Conduits Using Transit-Time Ultrasonic Flowmeters”, An American National Standard, 1994.

[10] M.F. Hamilton and D.T. Blackstock, Nonlinear Acoustics: Theory and Application, Academic Press, 1998.

[11] L.E. Kinsler, A.R. Frey, A.B. Coppens and J.V. Sanders, Fundamentals of Acoustics, John Wiley & Sons, 3rd Ed., pp. 179,1982.

[12] FUNDAMENTALS OF ELECTROACOUSTICS, http://www.massa.com/fundamentals.htm

[13] L.C. Lynnworth, D.R. Patch and W.C. Mellish, “Impedance-Matched Metallurgically Sealed Transducer, IEEE Transactions on Sonics and Ultrasonics, Vol. SU-31, pp. 101-104, 1984.

[14] P.M. Morse and K.U. Ingard, Theoretical Acoustics, Chapter 11, Princeton, 1986.

[15] B.N. Taylor and C.E. Kuyatt, *Guidelines for Evaluating and Expressing the Uncertainty of NIST Measurement Results*, NIST Technical Note 1297, 1994.

[16] Markham, Beyer and Lindsay "Review of Modern Physics" 23**,** 353 .(1951)

[17] SG Ejakov, S Phillips, Y Dain, RM Lueptow, and JH Visser, “Acoustic attenuation in gas mixtures with nitrogen: Experimental data and calculations”, JASA 113(4) Pt1 1871-1879.

[18] L. Shen, PhD, “Numerical Simulation for Low Velocity Air Flow Exposed to Solar Radiation”, GE Sensing report, pp. 1-12, 2010.

[19] S. Ao, PhD, J. Matson, O. Khrakovsky, “Wetted and Clamp-on Gas Flow Meter under Harsh Conditions”, GE Sensing report, pp 21-25, 2010.